Apoptosis (2019) 24:529–537
https://doi.org/10.1007/s10495-019-01531-1

Improved in vivo targeting of BCL-2 phenotypic conversion through hollow gold nanoshell delivery

Erin Morgan[1] · John T. Gamble[2] · Martin C. Pearce[2] · Daniel J. Elson[2] · Robert L. Tanguay[2,3,4] · Siva Kumar Kolluri[2,3,4] · Norbert O. Reich[1]

Published online: 16 March 2019

Abstract

Although new cancer therapeutics are discovered at a rapid pace, lack of effective means of delivery and cancer chemoresistance thwart many of the promising therapeutics. We demonstrate a method that confronts both of these issues with the light-activated delivery of a Bcl-2 functional converting peptide, NuBCP-9, using hollow gold nanoshells. This approach has shown not only to increase the efficacy of the peptide 30-fold in vitro but also has shown to reduce paclitaxel resistant H460 lung xenograft tumor growth by 56.4%.

Keywords Peptide delivery · Bcl-2 · Hollow gold nanoshells · Apoptosis · Resistant cancer · NuBCP

Introduction

Despite many advances, cancer is still a leading cause of death worldwide. Traditional chemotherapy is based largely on small molecule anti-cancer drugs which, although effective, have severe drawbacks including lack of specificity, high toxicity and often result in drug resistance, precluding continued use [1, 2]. The recently developed biologics have improved specificity, in some cases targeting tumors that develop resistance to small molecule therapies [3]. Resistant cancer cells often remain after initial chemotherapy treatment causing tumor recurrence. These resistant cancer cells can be specifically targeted through delivery of a pro-apoptotic peptide, fused with a poly arginine cell penetrating peptide [4]. Although delivery of pro-apoptotic peptides have shown great promise as new therapeutics, major delivery obstacles still thwart their progress in the therapeutic pipeline.

Intracellular delivery of apoptotic peptides through fusion to cell penetrating peptides like poly arginine, often results in endosomal entrapment [5]. This prevents the drug from reaching the cytosol as well as the subcellular target, in this case, the mitochondria [5]. The low efficiency of endosomal escape makes these therapeutic peptides efficient only at micromolar ranges in vitro [4]. Although the IC_{50} value in vitro cannot be directly correlated to activity of a therapeutic in vivo, therapeutics with an IC_{50} value > 10 μM are generally considered weak with a lower potential for in vivo application [6]. In order to increase the potency of therapeutics with high potential, a safe yet efficient delivery vehicle is required.

Here we demonstrate a hollow gold nanoparticle (HGN)-based intracellular delivery platform that overcomes many of these challenges. Orthogonal assembly of a Bcl-2 targeting peptide is achieved via thio-gold bonds; treatment of the HGN construct with pulsed near infra-red (NIR) light results in the release of the Bcl-2 targeted peptide. The Bcl-2 family of proteins regulate cell death via both pro-apoptotic and

Erin Morgan and John T. Gamble contributed equally.

Electronic supplementary material The online version of this article (https://doi.org/10.1007/s10495-019-01531-1) contains supplementary material, which is available to authorized users.

✉ Erin Morgan
emorgan@chem.ucsb.edu

✉ Norbert O. Reich
reich@chem.ucsb.edu

[1] Department of Chemistry and Biochemistry, University of California, Santa Barbara, CA, USA

[2] Department of Environmental and Molecular Toxicology, Oregon State University, Corvallis, OR, USA

[3] Linus Pauling Institute, Oregon State University, Corvallis, OR 97331, USA

[4] Center for Genome Research and Biocomputing, Oregon State University, Corvallis, OR 97331, USA

anti-apoptotic pathways and are now established as promising therapeutic targets in lymphoma and triple negative breast cancer (TNBC) [7, 8]. Expression of Bcl-2 in hormone receptor-negative and TNBC cancers is an independent poor prognostic factor and associated with poor outcome in patients treated with anthracycline based adjuvant chemotherapy [9, 10]. Upregulation of Bcl-2 is a mechanism of therapeutic resistance in HER2-positive and TNBC which contributes to poor overall survival [11, 12].

Current strategies targeting Bcl-2 include peptides derived from the BH3 domain and small molecule inhibitors such as ABT-199 and ABT-737. However, resistance to ABT-199 is linked to upregulation of other anti-apoptotic proteins such as Bcl-xL [13, 14]. An alternative approach to target Bcl-2 in TNBC is the use of NuBCP-9 (NuBCP) which is a nine amino acid peptide derived from Nur77 [15, 16]. Bcl-2 binding of NuBCP converts it into a pro-apoptotic protein. NuBCPs' action is potentiated by increased Bcl-2 expression and is capable of inhibiting the pro-survival function of Bcl-xl which is linked to ABT-199 resistance mechanisms [17, 18]. However, the delivery of NuBCP is problematic due to its biodegradation and short circulation half-life. Prior efforts to improve on NuBCP delivery still required micromolar concentrations [19–21].

The use of gold nanoparticles as a delivery vehicle for peptide delivery, such as NuBCP, has the potential to increase the potency of NuBCP through increased endosomal escape upon NIR irradiation. The light triggered release of NuBCP also enables specific release in a target area so the resistant cancer cells can be targeted systematically while leaving other tissues untouched.

Materials and methods

Hollow gold nanoshell synthesis and dialysis

HGNs were synthesized through a previously described galvanic replacement of silver seed particles [22]. Briefly, the synthesis can be broken into three steps. The first step initializes the silver seed of the particle in a 500 mL solution of 0.2 mM $AgNO_3$ (Sigma) and 0.5 mM sodium citrate (Sigma) heated to 60 °C. 0.5 mL of 1.0 M $NaBH_4$ (EMD) was added quickly to reduce the silver solution to create the initial silver seed. The solution remained at temperature for 2 h and then left to cool to room temperature. The second step of the synthesis grows the silver particle to the final 45 nm size by the addition of 0.75 mL of 2 M $NH_2OH{\cdot}HCl$ (Sigma) and 1.75 mL of 0.1 M $AgNO_3$. The solution stirred overnight to allow for full growth of the silver particles to be used for template for later galvanic replacement. The third and final step in the synthesis is the galvanic replacement of the sacrificial silver template by the addition of 3.2 mL of 25 mM $HAuCl_4$ (Sigma) to the heated solution at 60 °C to obtain hollow gold nanoshells ~ 45 nm in diameter with an absorption peak maximum at 750 nm. The HGNs were dialyzed overnight in sodium citrate buffer (500 mM) with 0.03% diethyl dicarbonate (DEPC) (Biochemica) in dialysis cassettes (MWCO 20 kDa).

HGNs surface modifications

DNA adsorption

Thiol–PEG–DNA–amine C_6-S-S-PEG_{18}-5′ ACCCTGAAG TTCATCTGCACCACCG-3′-NH_2 (100 µM, Biosearch Technologies) was deprotected through a 20 min incubation with 12.5 mM Tris(2-carboxyethyl)phosphine hydrochloride (TCEP, Sigma). A chloroform extraction was performed to remove the C_6 cap on the 5′ end of the oligo. 6 µM of TCEP treated DNA was added to 64 pM HGN. After a brief sonication, 10 mM sodium citrate was added to adjust the pH of the solution to 3.1 in order to allow for low pH DNA adsorption onto the surface of the HGN. After 20 min of incubation at a low pH, the pH was raised to 7.4 with 1 M HEPES (Sigma) and the solution was slowly salted to 1 M Na^+ over a period of 20 min using 3.0 M sodium chloride (NaCl), 0.3 M sodium citrate (Na_3Cit) pH 7.0 (SSC 20×) with 0.01% Tween-20 and 1 mM $MgCl_2$. After another 20-min incubation excess DNA was through two wash steps performed by centrifuging at 10,000 x g for 10 min with resuspension and sonication in washing buffer (1 mM $MgCl_2$, 0.01% Tween-20, 300 mM NaCl and 30 mM Na_3Cit pH 7). After the last wash, the particles were suspended in hybridization buffer (10 mM $MgCl_2$, 600 mM Na^+).

Hybridization of complementary DNA

Complementary DNA (2 µM) is added to the HGN–DNA in ratio of 1:9 (5′-biotin to 5′-FAM labeled) to allow for a varied surface modification of the HGN. 0.2 µM biotin and 1.8 µM DNA_{comp}-FAM are added to hybridization buffer, mixed and then added to 64 pM HGN–DNA to a final concentration of 1 µM complement DNA with 32 pM HGN–DNA and sonicated. The solution is then heated at 70 °C for 2 min and held at 45 °C for 30 min before washed two times with conjugation buffer (10 mM HEPES, 1 mM $MgCl_2$ and 0.01% Tween-20).

NTA functionalization of HGN–DNA

N-[*N*α,*N*α-Bis(carboxymethyl)-L-lysine]-12-mercaptododecanamide (NTA) (Sigma) was added to the amine at the 3′ end of the dsDNA strand through a 20 min room temperature incubation with 1 mg mL^{-1} NHS–PEG_4–maleimide linker (Quanta Biodesign). After

20 min the maleimide terminated HGN–DNA particles were washed three times at 4 °C and then suspended in conjugation buffer with 50 μM NTA, sonicated and left at room temperature for 3 h and then washed three times in PBS with 0.01% Tween-20 (PBST).

Streptavidin and biotin–TAT functionalization of HGN–NTA

An equal volume of 1 mg mL^{-1} streptavidin (Prozyme) in PBST was added to 62 pM HGN–NTA and quickly sonicated and vortexed. After 1 h of incubation at room temperature the streptavidin coated HGN were centrifuged twice at 10,000 × g for 10 min at 4 °C and each time was suspended in PBST. A final concentration of 20 μM biotin-TAT (Anaspec) was added in two steps of equal volume with a 30 min incubation at room temperature after each addition. The particles were then washed another two times with PBST to remove any excess biotin–TAT and stored at 4 °C until further use.

NuBCP loading onto HGN and quantification of loading

NuBCP was loaded onto the HGN at 1, 3 and 10 μM initial concentration for 32 pM HGN and 500 μM $CuCl_2$ and incubated for 20 min on ice before being washed three times in PBST. Total loading per particle was determined through KCN etch. 32 pM particles were incubated in KCN solution [0.1 M KCN, 1 mM $K_3Fe(CN)_6$] to dissolve the gold particles and completely release the molecules coating the particle surface. In laser experiments, quantification of peptide released by laser was determined after centrifugation of the lasered sample and removal of the supernatant. The pellet was treated with KCN etch to determine the amount retained on the particle. Quantification of peptide in the supernatant and etched off the pellet was determined using standard linear calibration curves between concentration of Cy5 labeled NuBCP and the corresponding fluorescence intensity detected from the Tecan M200 plate reader. The fluorescence intensity in solution released with KCN etch or laser irradiation was converted to peptide concentration using the calibration curve.

Two-photon microscopy

Cells were plates 24 h prior at 40,000 cells per well in an 8 well glass slide (Millipore cat no. PEZGS0816) in 200 μL of DMEM + 10% FBS. 500 μM $CuCl_2$ was added to 25 μL of ~ 32 pM HGNs (in PBST) prior to addition of NuBCP-Cy5. Particles were sonicated and incubated with 1, 3 and 5 μM NuBCP-Cy5 for 30 min on ice then spun down at 5000 rcf for 10 min and washed 1 × with PBST. HGN–NuBCP-Cy5 particles were then suspended in 200 μL of DMEM + 10% FBS and sonicated prior to addition to 8 well glass slide for 2 h at 37 °C in 5% CO_2. Cells were washed 2 × with PBS and then one drop of PBS was added to each well prior to cover glass addition. Samples were focused on using a 25 × water immersion objective lense and irradiated using a mode locked Ti:sapphire tunable femtosecond pulsed laser (100 fs pulse duration, 80 mHz repetition rate, Mai Tai HP, Newport-Spectra Physics). The excitation source was set to irradiate at 800 nm, 5% NIR laser power and in 0.69 nm slices throughout the cell volume. Images capturing FAM and Cy5 fluorescence were collected before and after laser irradiation.

Cellular internalization and imaging

Cells were plated and treated with HGN, HGN + NuBCP (containing no DNA or TAT),HGN–DNA–NuBCP, HGN–DNA–TAT, HGN–DNA–TAT–NuBCP, or no particles as described above and observed on an Olympus BX51 upright compound microscope with a dark field condenser.

Mitochondrial depolarization assay of cancer therapeutic resistant H460 cells treated with HGN and HGN–NuBCP

Cells were plated and treated with HGN or HGN–NuBCP as described above. Prior to irradiation, cells were treated with media containing 10 μg mL^{-1} solution of JC-1 dye (ThermoFisher) and incubated for 10 min. The cells were washed three times with PBS and treated with the laser conditions outlined above.

Femtosecond pulse laser irradiation of HGN in MDA-MB-231 cells through microcapillary device

MDA-MB-231 cells were dissociated from flask using cell dissociation buffer (CDB, Gibco), and washed two times with PBS. 100,000 cells were suspended in media and incubated for 2 h with HGN and HGN–NuBCP. The cells were washed two times with PBS and divided into 5000 per tube in 100 μL and focused through a capillary tube positioned perpendicular to the NIR beam path at a rate of 100 μL min^{-1}. Samples without irradiation were passed through the capillary tube with NIR beam path blocked to prevent irradiation of the sample. The samples were collected and plated on a 96 well plate and assayed for viability 96 h later using the PrestoBlue viability stain according to the manufacturer's protocol on a Tecan M200 plate reader.

Zebrafish xenograft and two-photon laser exposure

Zebrafish (*Danio rerio*) housing was conducted at the Sinnhuber Aquatic Research Laboratory at Oregon State University in accordance with Institutional Animal Care and Use Committee protocols. Under standard laboratory conditions, adult 5D tropical zebrafish were maintained at 28 ± 1 °C on a 14 h light/10 h dark photoperiod in reverse osmosis water with added salt solution (0.6%, Instant Ocean, UnitedPet Group, Inc., Blacksburg, VA, USA). Eggs collected were staged according to Kimmel et al. [23]. To prevent pigmentation, zebrafish embryos were maintained in E3 media with phenylthiourea (0.003%, Sigma, USA) starting at 24 h post fertilization.

Before transplantation, cancer cells were labeled with a CM-DiI cell tracker dye (ThermoFisher Science) according to the manufacturer's protocol and exposed to vehicle (media), HGN 32 pM or HGN–NuBCP 32 pM loaded with 10 μM treatment. Cells were allowed to incubate with treatment at room temperature for 1 h on a rotator. Cells were then washed with PBS and suspended in DMEM to a concentration of 2×10^7 cells mL^{-1}. Xenograft transplantation occurred as in Pearce et al. [4]. Briefly, suspended cells were loaded into a glass needle pulled from a borosilicate glass pipette by a micropipette puller (Sutter Instrument, Novato, CA). Around 200 cancer cells were transplanted into the yolk of 2-day post fertilization zebrafish by a micro-pressure injector. Xenografts recovered overnight at 34 °C without light after transplantation.

For two-photon laser irradiation, zebrafish were immobilized by being anesthetized by emersion in 0.2 mg mL^{-1} Tricaine E3 media and imbedded in 0.8% (w/v) low melting point agarose on a glass bottom 96-well plate. Zebrafish were irradiated using a mode locked Ti:sapphire laser widely tunable femtosecond pulsed laser (140 fs pulse duration, 80 mHz repetition rate, Chameleon Vision Laser, Coherent) using a Zeiss LSM 780 confocal microscope at ×20 objective. Zebrafish yolks were irradiated at 800 nm, 6% NIR laser power and in 0.75 nm slices throughout the yolk volume.

For imaging, zebrafish xenografts at 1 and 4-day post injection (dpi) were immobilized as mentioned above and fluorescent cells were captured on a as z-stacks with wide-field settings on a Zeiss LSM 780 confocal microscope with a ×10 objective. Using Fiji (ImageJ) software, cancer growth was analyzed by producing a maximum projection image of a median filtered z-stack and calculating the cell area from an Otsu applied threshold [24]. An increase in cell area from 1 to 4 dpi was consider cancer growth.

Results

To assemble the HGN–peptide constructs, single strands of thiol–DNA–amine were added to the surface of the HGN through low pH mediated adsorption followed by addition of a complementary DNA strand. The complementary DNA strand allows for tracking of the particles (with FAM-tagged DNA) and internalization through a DNA-biotin tag. A ratio of 1:9 (biotin:FAM) allows for optimal peptide loading onto the HGN (~ 10,000 peptides/particle) with efficient internalization (Fig. S1a). The biotin strand allows for internalization into cells only after the addition of streptavidin and a biotinylated cell penetrating peptide, TAT (Biotin-YGRKKRRQRRRPQ). The terminal amine on the thiol–DNA anchoring strand was further functionalized with a thiol derivative of nitrilotriacetic acid (NTA) using a NHS–PEG4–maleimide linker. The NTA on the surface of the particle allows for the His-tagged NuBCP onto the particle in the presence of Cu^{2+} (Fig. 1a). The average diameter of the final construct increased from 58 to 190 nm from citrate capped HGN to the full construct containing NuBCP (Fig. 1b). Figure 1c demonstrates the delivery of HGN–NuBCP via streptavidin TAT mediated endocytosis. After irradiation with 800 nm light, NuBCP is released from the HGN and the endosome into the cytosol. Upon release, NuBCP binds to the Bcl-2 loop domain and converts Bcl-2 into a pro-apoptotic protein, which further inhibits anti-apoptotic proteins and activates other pro-apoptotic proteins on the mitochondria. Finally, activated pro-apoptotic proteins facilitate mitochondrial outer membrane permeabilization, initiating apoptosis, resulting in cell death [16].

In order to verify the HGN–NuBCP construct has laser-controlled release of NuBCP, both cell-free and cell-based release studies were conducted. Cell-free treatment shows laser-dependent release of the peptide with up to 22% of the loaded peptide (Fig. 2a). Total loading of the peptide was determined through Cy5 fluorescence following a KCN etch of the washed HGN–NuBCP pellet (Fig. S1b) level of release is typical for peptides and proteins loaded onto HGNs [4]. Cellular internalization of nanoparticles containing TAT was observed via dark field microscopy (orange puncta Fig. 2b). Initial release experiments in HeLa cells using two-photon microscopy also demonstrates internalization of the HGN–peptide constructs visualized as fluorescent puncta within the endosomes as seen in the lower left panel of Fig. 2c. Only after NIR irradiation was release of the FAM labeled DNA as well as the NuBCP-Cy5 observed as the puncta diffused across the cell demonstrating endosomal release (Fig. 2c). Similar experiments were carried out with MDA-MB-231 breast cancer cells that express high levels of Bcl-2 (Fig. 3a, b).

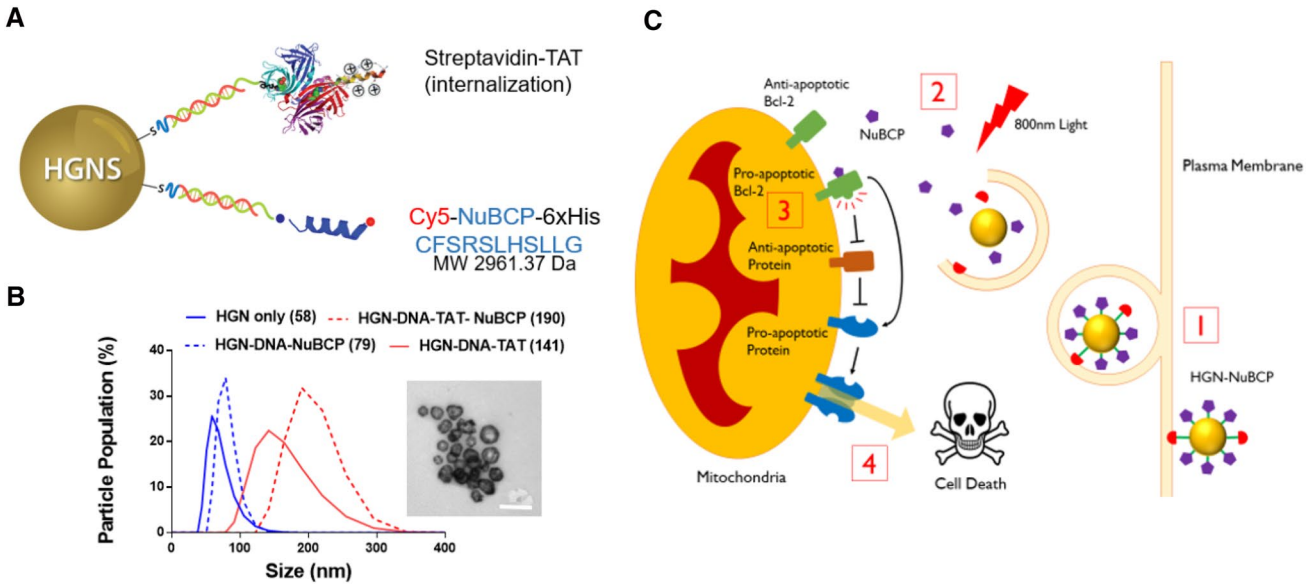

Fig. 1 **a** Orthogonal surface chemistry of internalization peptide streptavidin TAT and therapeutic peptide NuBCP-9 on a HGNs. **b** Size distribution of nanoparticles during coating steps. HGN particles have a Z-average diameter of 58 nm; HGN–DNA-, 79 nm; HGN–DNA–TAT, 141 nm; HGN–DNA–TAT–NuBCP-9, 190 nm. Image to the right displays TEM image of HGN–DNA–TAT. Scale bar 100 nm. **c** Illustration of the delivery of HGN–NuBCP-9 into a cancer cell. (*1*) Hollow gold nanoparticles coated in NuBCP-9 (purple hexagon) are taken into the cell by internalization peptide streptavidin TAT (red semi-circle) mediated endocytosis. (*2*) Irradiation with NIR 800 nm light, releases NuBCP-9 from nanoparticle and endosome into the cytosol. (*3*) NuBCP-9 binds to the Bcl-2 loop domain and converts Bcl-2 (green) into a pro-apoptotic protein which inhibits anti-apoptotic proteins (orange) and activates other pro-apoptotic proteins (blue) on the mitochondria. (*4*) Activated pro-apoptotic proteins facilitate mitochondrial outer membrane permeabilization, initiating apoptosis, and results in cell death. (Color figure online)

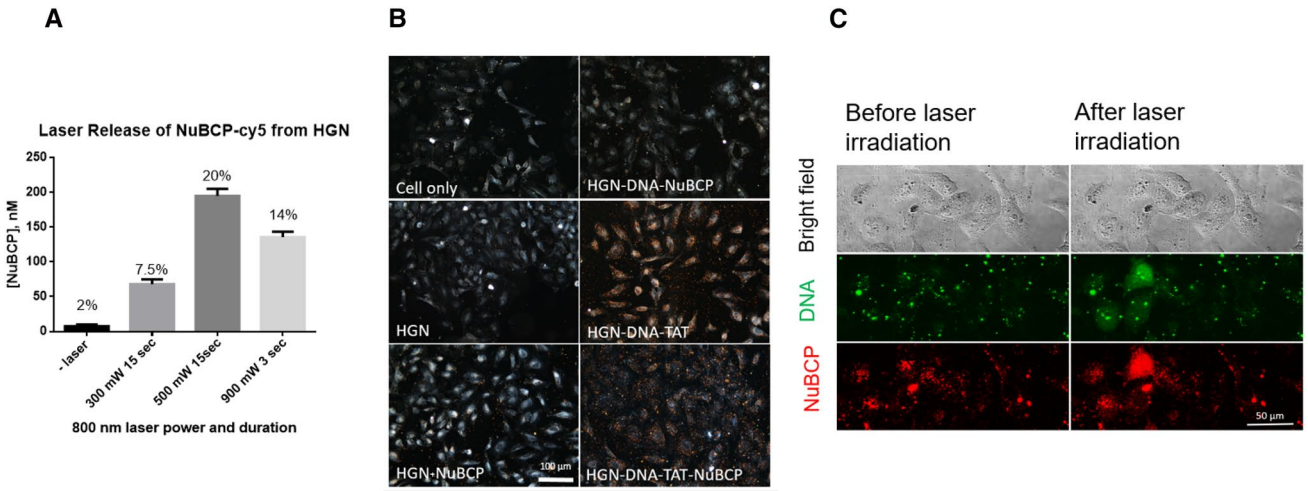

Fig. 2 Release of Cy5 labeled NuBCP shows laser dependent release. **a** An increase in laser power leads to an increase in NuBCP release from HGN loaded with 900 nM NuBCP. Percent release is shown above bar graphs and determined by the percentage of peptide released into the supernatant after laser irradiation. Total peptide loaded is determined by KCN etch of the no laser pellet. **b** HGN internalization is dependent on presence of TAT. Dark field microscopy demonstrates cellular internalization of gold nanoparticles (orange light scattering) only when TAT peptide is present on the particle surface. **c** Release of FAM labeled DNA and Cy5 labeled NuBCP in HeLa cells using two photon microscope for NIR laser irradiation. Release of both DNA and peptide is shown from diffusion of dye labels throughout the cell after laser irradiation

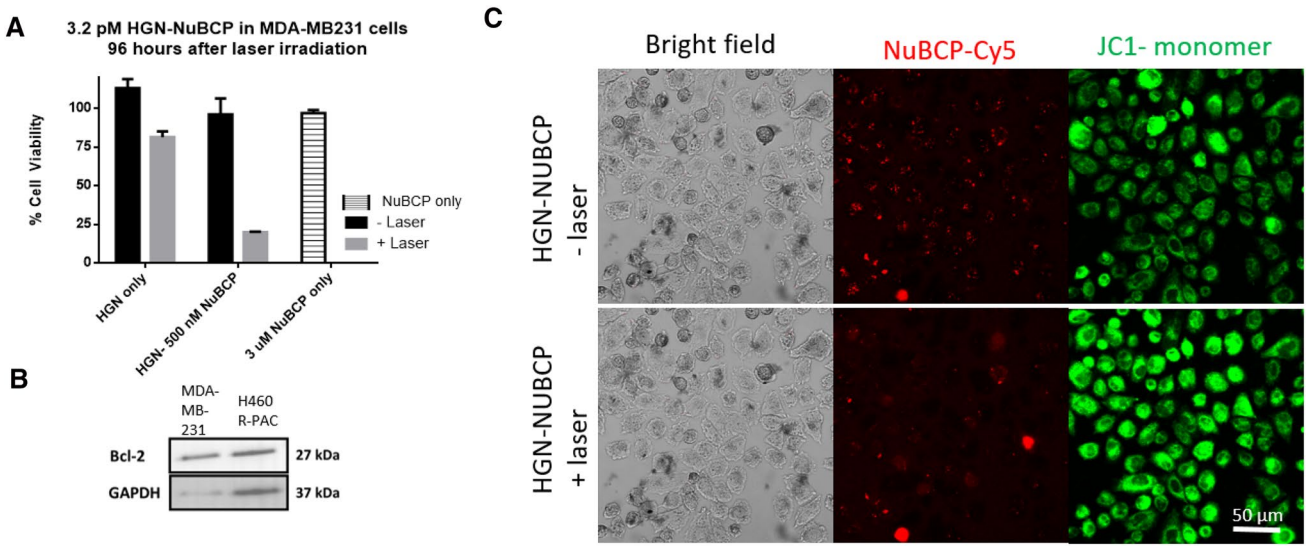

Fig. 3 **a** MDA-MB-231 cells were treated with 3.2 pM HGN, 3.2 pM HGN–NuBCP and were then irradiated with an 800 nm 5 kHz laser at 1 W as cells flowed through a borosilicate microcapillary tube at 100 µL min^{-1}. 500 nM and 3 µM NuBCP indicate the final concentration of NuBCP delivered in cell media via HGNs or in media alone for NuBCP only. Note the NuBCP only control was not treated with laser. Cell viability of MDA-MB-231 cells was observed 96 h after laser irradiation. **b** Bcl-2 is expressed in both MDA-MB-231 and H460 R-PAC cells. Western blot analysis of MDA-MB-231 and H460 R-PAC indicates levels of Bcl-2 and GAPDH is used as a loading control. **c** Laser dependent release of NuBCP-Cy5 in H460 cells with JC-1 assay shows mitochondrial destabilization as green fluorescence increases from the JC-1 monomer upon irradiation with two-photon 800 nm laser

Bulk laser experiments used a micro-capillary device to flow the cells with internalized particles through the path of the laser beam to maximize the fraction of cells exposed to irradiation [5]. Cell viability was determined 96 h after laser irradiation and demonstrated 80% cell viability loss with HGN–NuBCP particles. When MDA-MD-231 cells were treated with three times the amount of the unconjugated NuBCP peptide, the cells remained viable. This indicates the HGN particles are necessary for uptake of the peptide into the cells in order to cause the desired effect. A control involving HGN particles without NuBCP was irradiated with NIR light and a cell viability loss of only 10% was observed likely due to heating caused on the surface of the HGNs. This data demonstrates the requirement for both HGN and NuBCP for effective loss of cancer cell viability.

When an initial concentration of 10 µM NuBCP is incubated with 32 pM HGN, 1.8 µM is actually loaded onto the HGN construct (Fig. S1). After irradiation only 500 nM NuBCP is released from the particles in cell-free studies. This value can be used to estimate the maximum amount of NuBCP released and used for cell studies (50 nM). This data suggests our HGN–NuBCP delivery increases the potency of the peptide by 30-fold compared to previous particle delivery methods [19]. We observe no cell death when MDA-MB-231 cells are treated with the peptide without HGN assembly (Fig. 3a). The HGN–NuBCP in MDA-MB-231 cells showed no significant cell viability loss without laser irradiation indicating either the NuBCP remains attached on the HGN in the cellular endosomes or is degraded after 96 h.

To verify the cause of viability loss in cells expressing high levels of Bcl-2 was due to the induction of apoptosis, we tested the efficacy of the system in H460 lung cancer cells using the JC-1 mitochondrial stain to test for mitochondrial destabilization after irradiation of HGN–NuBCP particles (Fig. 3c). In cellular studies, aggregated JC-1 dye disassociates into a green fluorescing monomeric form when the mitochondrial membrane depolarizes. Mitochondrial depolarization can be an early indicator of cell death due to apoptosis. Confocal images show release of the NuBCP from HGN and the increase in green fluorescence form of the JC-1 monomers 30 min after irradiation with NIR light and release of NuBCP from the HGN (Fig. 2b). Only in areas with laser irradiation was an increase in green fluorescence observed, confirming the mitochondrial membrane becomes destabilized after irradiation of cells with HGN–NuBCP. There is no effect of HGN alone with laser on mitochondrial health (Fig. S2). These findings show NuBCP can be delivered into human cancer cells where release of the NuBCP from the gold particles leads to a compromised mitochondria membrane.

To determine any potential toxicity of HGN–NuBCP-9 to normal cells we performed zebrafish toxicity and survival assay (Fig. 4a). Exposure of HGN–NuBCP did not impact survival or development of abnormalities of zebrafish embryos. To demonstrate the in vivo efficacy of

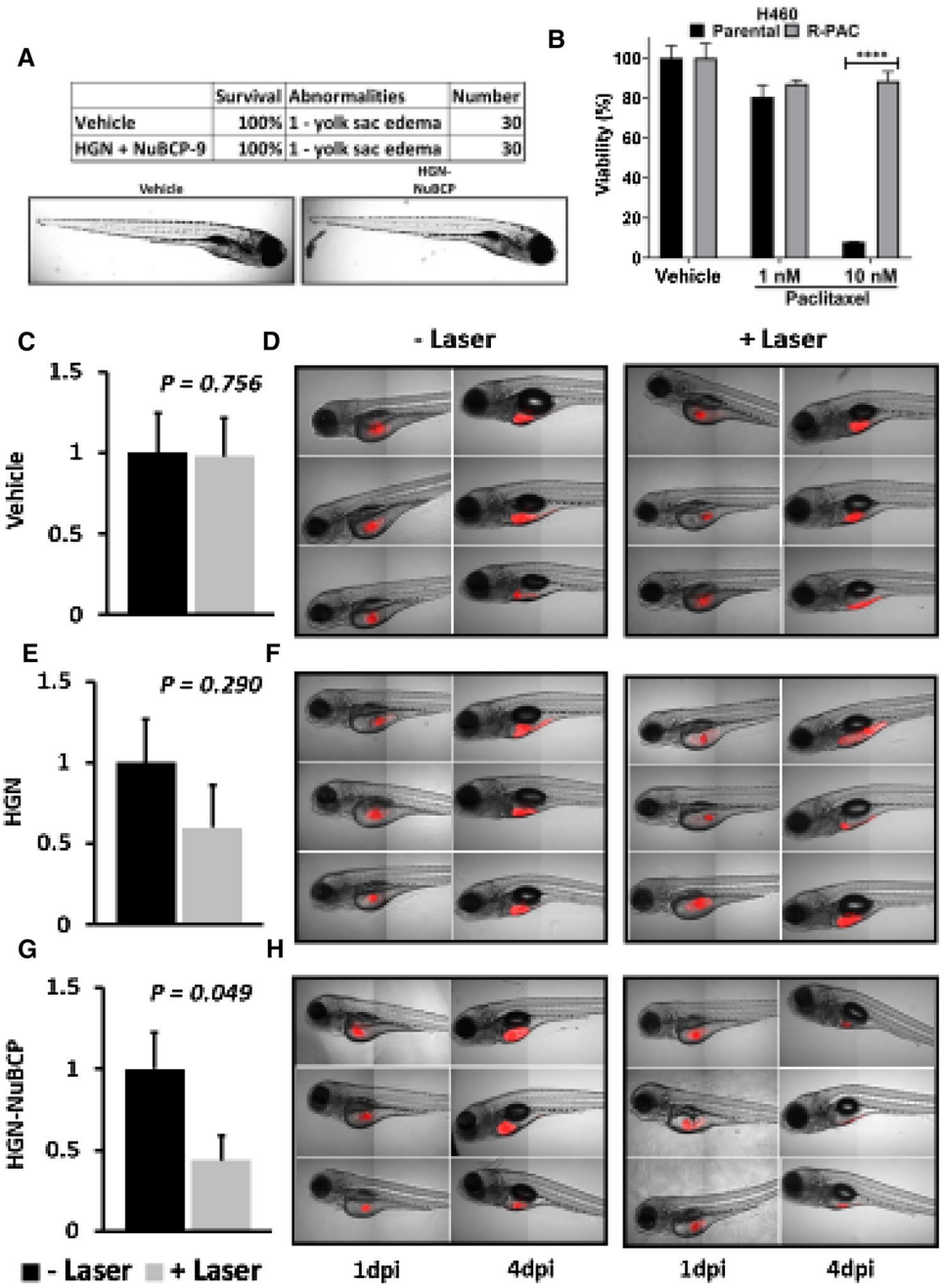

Fig. 4 **a** Effect of HGN–NuBCP-9 on survival and development of zebrafish embryos. Treatment with vehicle (PBS–Tween 0.01%) and HGN–NuBCP-9 10 μM in embryo media. Survivorship was assessed by counting the number of live versus dead fish in each group (N = 30 all groups). **b** H460 derived paclitaxel line is resistant to 10 nM paclitaxel treatment. Percentage viability is calculated relative to vehicle treatment. Data is representative of three independent assays done in triplicate. Two-way ANOVA with Sidak's multiple comparisons post-test, ****P < 0.0001. Log2 fold change of cell area for vehicle (**c**), HGN (**e**) and HGN–NuBCP (**g**) exposed H460 PacR cells in xenografts after no exposure (−Laser) or exposure (+Laser) to two-photon NIR laser. Data normalized to no laser control; vehicle (−Laser) N = 20, (+Laser) N = 20: HGN: (−Laser) N = 20, (+Laser) N = 19. HGN–NuBCP: (−Laser) N = 19, (+Laser) N = 20. Representative figures zebrafish xenografts for vehicle (**d**), HGN (**f**) and HGN–NuBCP (**h**) treatment groups at 1 and 4 day post injection (dpi) with transplanted H460 PacR cells (red); ×10 magnification. (Color figure online)

this HGN–NuBCP approach, we exposed paclitaxel resistant (PacR) H460 cells to either vehicle, HGN, or HGN–NuBCP and transplanted them into zebrafish embryos (Fig. 4). H460 cells were systematically exposed to low doses of paclitaxel, resulting in increased Bcl-2 expression and resistance to paclitaxel (PacR H460 cell line) [4]. The H460 paclitaxel PacR cells derived from H460 parental cells are 10-fold less sensitive to paclitaxel than the parental cells at 10 nM paclitaxel, which is a clinically achievable concentration (Fig. 4b). The transplanted cells were imaged before and 3 days after two-photon NIR laser irradiation to measure loss of PacR H460 cells within the zebrafish. Half the zebrafish from each group were withheld from irradiation as controls. NIR irradiation had no effect on zebrafish survival as 98.3% and 96.6% of non-irradiated and irradiated zebrafish survived respectively. Laser irradiation of HGN–NuBCP treatment group had the greatest effect on the growth of PacR H460 cells inside zebrafish. Three days after laser irradiation, average PacR H460 xenograft tumor growth was reduced by 56.4% compared to the non-laser control for HGN–NuBCP treated groups (Fig. 4g, h). PacR H460 xenograft growth was not significantly affected by the media used for delivery (Fig. 4c, d) nor HGN alone (Fig. 4e, f). Laser induced cell reduction with HGN exposure is similar

to what was seen in vitro experiments where HGN irradiation may be generating localized heating.

Discussion

Our primary interests were the induction of apoptosis in resistant cancer cells with NIR light control and to limit the amount of peptide required in therapeutic applications. Successful cancer therapies rely significantly on both the selectivity for cancer cells as well as creating a reasonable therapeutic window for in vivo studies. The Nur77 derived peptide, NuBCP targets Bcl-2 and converts it into a pro-apoptotic protein as well as inhibits the pro-survival function of Bcl-xl [17, 18]. Therefore, delivery of NuBCP with hollow gold nanoshells would not only allow for control over release with light but the peptide itself would affect the cells that are resistant to traditional Bcl-2 targeting therapeutics [17, 18]. Earlier studies using the Nur77 derived peptide, NuBCP required high micromolar concentration of peptide in order to cause apoptosis which can translate to poor efficacy in vivo [19–21]. Our hypothesis was that addition of the NuBCP to hollow gold nanoshells would improve the delivery efficiency since peptides delivered solely via targeting peptides are often caught in endosomes [5].

Our research demonstrates the release of the NuBCP peptide from our HGN construct with 800 nm light control (Fig. 3a). In Fig. 2a the power dependence of release is observed after different laser intensities are applied to the HGN containing NuBCP with a Cy5 dye. This suggests that the peptide is not released from the particle until a certain power of excitation is obtained. Since up to 20% of the loaded peptide was released from the HGN after laser irradiation, this would convert to a maximum of 50 nM NuBCP delivered in cellular studies. Furthermore, NuBCP laser dependent release from the HGN in cells is visualized by the diffusion of the dye attached to the peptide after laser irradiation (Fig. 2c). Tracking of the DNA also attached to the particle is seen through the FAM fluorescence channel and shows that cells that release NuBCP also show the dispersion of DNA-FAM confirming that the NuBCP peptide is attached to the particle via the NTA–Cu–His interaction originally hypothesized.

Release of the NuBCP peptide from HGN not only showed significant cell death in MDA-MB-231 breast cancer cells (Fig. 3a) but also that the overall peptide quantity required with HGN–NuBCP is 30-fold less than those previously delivery methods of NuBCP [19]. Active mitochondria can give insight to early apoptosis through the JC-1 assay, which detects membrane depolarization of the mitochondria. Our data in Fig. 3c suggests that only upon irradiation with NIR light does the HGN–NuBCP cause disruption of the mitochondria membrane, via enhancement of the green fluorescence overtime. Control studies with NIR light and HGN without the NuBCP peptide showed no change in the mitochondria health (Fig. S2). The JC-1 assay studies were conducted in the H460 (PacR) cell line. Bcl-2 is highly expressed in non-small cell lung cancer and TNBC (Fig. 3b), therefore NuBCP-9 targeting of Bcl-2 is not limited to one cancer type but will be effective in cancer subtypes expressing Bcl-2.

Finally, these results were translated to in vivo efficacy studies with HGN–NuBCP in zebrafish embryos. Embryo-larval zebrafish are highly sensitive to environmental factors during development. Zebrafish have been successfully used as model for assessing potential human toxicity with high sensitivity, including nanoparticles and therefore are uniquely qualified for initial testing to assess the safety of developing new drugs [25, 26]. Moreover, the excellent transparency of the larval zebrafish allowed elucidation of the proper laser power as visualization of HGN resonant light intensity was used to confirm that the proper laser power was reaching the cancer cells within the zebrafish [27, 28]. Paclitaxel resistant (PacR) H460 cells were exposed to HGN–NuBCP and transplanted into zebrafish embryos, which were treated with NIR light. The NIR light allowed for release of the Bcl-2 targeting NuBCP and reduced the tumor growth in these samples by 56.4% compared to the non-laser control for HGN–NuBCP (Fig. 4g, h). This indicates not only that the HGN-delivery method can be used for peptide delivery in vivo, but also that the release of the NuBCP from the HGN is light controlled in this system as well.

Conclusion

In conclusion, we report the use of HGN for the delivery of a Bcl-2 functional converting apoptotic peptide, NuBCP, to therapeutic resistant cells. Laser controlled HGN delivery of NuBCP not only drives down the therapeutic dose required of NuBCP to induce apoptosis by 30-fold, it also provides a means to target tumor-specific regions. Laser release was shown to be safe and effective for reducing chemotherapy resistant tumor growth in zebrafish xenografts. Our results suggest the light control of NuBCP with HGN not only increased efficacy in vitro but the efficiency in vivo demonstrates the potential application of HGN–NuBCP as a therapeutic to treat cancers that express Bcl-2.

Acknowledgements This work was supported by the National Institutes of Health (NIH) Grant R01 EB012637 and in part by Grants from the US Army Medical Research and Material Command (W81XWH-08-1-0600 and W81XWH-12-1-0069), American Cancer Society (RSG-13-132-01-CDD), National Institutes of Health (5RO1ES016651) and Oregon State University Venture Development Fund (http://advantage.oregonstate.edu/funding-opportunities). The

authors thank support of the NRI Microscopy Center, the Olympus confocal microscope was funded by the NIH Grant 1S10RR022585-01A1. The authors thank A. Mikhailovsky for helpful conversations and aid of the UCSB Optical Characterization Facility. The ultrafast laser system was funded by DURIP ARO Grant 66886LSRIP. The authors would also like to thank former graduate student Demosthenes Morales for helpful discussions.

Compliance with ethical standards

Conflict of interest The authors declare no competing financial interests.

References

1. Allen TM (2002) Ligand-targeted therapeutics in anticancer therapy. Nat Rev Cancer 2(10):750–763
2. Holohan C, Van Schaeybroeck S, Longley DB, Johnston PG (2013) Cancer drug resistance: an evolving paradigm. Nat Rev Cancer 13(10):714–726
3. Gupta D, Kumar M, Tyagi P, Kapoor S, Tyagi A, Barman TK et al (2018) Corrigendum to 'Concomitant delivery of paclitaxel and NuBCP-9 peptide for synergistic enhancement of cancer therapy' NANO 14 (2018) 1301–1313. Nanomed Nanotechnol Biol Med 14(7):2129
4. Pearce MC, Gamble JT, Kopparapu PR, O'Donnell EF, Mueller MJ, Jang HS et al (2018) Induction of apoptosis and suppression of tumor growth by Nur77-derived Bcl-2 converting peptide in chemoresistant lung cancer cells. Oncotarget. https://doi.org/10.18632/oncotarget.25437
5. Li H, Nelson CE, Evans BC, Duvall CL (2011) Delivery of intracellular-acting biologics in pro-apoptotic therapies. Curr Pharm Des 17(3):293–319
6. Hughes J, Rees S, Kalindjian S, Philpott K (2011) Principles of early drug discovery: principles of early drug discovery. Br J Pharmacol 162(6):1239–1249
7. Czabotar PE, Lessene G, Strasser A, Adams JM (2014) Control of apoptosis by the BCL-2 protein family: implications for physiology and therapy. Nat Rev Mol Cell Biol 15(1):49–63
8. Yip KW, Reed JC (2008) Bcl-2 family proteins and cancer. Oncogene 27(50):6398–6406
9. Bouchalova K, Svoboda M, Kharaishvili G, Vrbkova J, Bouchal J, Trojanec R et al (2015) BCL2 is an independent predictor of outcome in basal-like triple-negative breast cancers treated with adjuvant anthracycline-based chemotherapy. Tumour Biol J Int Soc Oncodev Biol Med 36(6):4243–4252
10. Honma N, Horii R, Ito Y, Saji S, Younes M, Iwase T et al (2015) Differences in clinical importance of Bcl-2 in breast cancer according to hormone receptors status or adjuvant endocrine therapy. BMC Cancer 15(1):698
11. Giuliano M, Hu H, Wang Y-C, Fu X, Nardone A, Herrera S et al (2015) Upregulation of ER signaling as an adaptive mechanism of cell survival in HER2-positive breast tumors treated with anti-HER2 therapy. Clin Cancer Res Off J Am Assoc Cancer Res 21(17):3995–4003
12. Real PJ, Sierra A, De Juan A, Segovia JC, Lopez-Vega JM, Fernandez-Luna JL (2002) Resistance to chemotherapy via Stat3-dependent overexpression of Bcl-2 in metastatic breast cancer cells. Oncogene 21(50):7611–7618
13. Choudhary GS, Al-harbi S, Mazumder S, Hill BT, Smith MR, Bodo J et al (2015) MCL-1 and BCL-xL-dependent resistance to the BCL-2 inhibitor ABT-199 can be overcome by preventing PI3K/AKT/mTOR activation in lymphoid malignancies. Cell Death Dis 6(1):e1593
14. Yecies D, Carlson NE, Deng J, Letai A (2010) Acquired resistance to ABT-737 in lymphoma cells that up-regulate MCL-1 and BFL-1. Blood 115(16):3304–3313
15. Lin B, Kolluri SK, Lin F, Liu W, Han Y-H, Cao X et al (2004) Conversion of Bcl-2 from protector to killer by interaction with nuclear orphan receptor Nur77/TR3. Cell 116(4):527–540
16. Kolluri SK, Zhu X, Zhou X, Lin B, Chen Y, Sun K et al (2008) A short Nur77-derived peptide converts Bcl-2 from a protector to a killer. Cancer Cell 14(4):285–298
17. Bodo J, Zhao X, Durkin L, Souers AJ, Phillips DC, Smith MR et al (2016) Acquired resistance to venetoclax (ABT-199) in positive lymphoma cells. Oncotarget 7(43):70000–70010
18. Huang S, Jiang C, Guo H, Wang J, Liu Y, Li C, Lopez E, Zhang H, Lorence EA, Merolle M et al (2017) Resistance mechanisms underlying venetoclax resistance in mantle cell lymphoma. Blood 130(Suppl 1):2749
19. Kapoor S, Gupta D, Kumar M, Sharma S, Gupta AK, Misro MM et al (2016) Intracellular delivery of peptide cargos using polyhydroxybutyrate based biodegradable nanoparticles: studies on antitumor efficacy of BCL-2 converting peptide, NuBCP-9. Int J Pharm 511(2):876–889
20. Kumar M, Gupta D, Singh G, Sharma S, Bhat M, Prashant CK et al (2014) Novel polymeric nanoparticles for intracellular delivery of peptide cargos: antitumor efficacy of the BCL-2 conversion peptide NuBCP-9. Cancer Res 74(12):3271–3281
21. Kumar M, Singh G, Sharma S, Gupta D, Bansal V, Arora V et al (2014) Intracellular delivery of peptide cargos using iron oxide based nanoparticles: studies on antitumor efficacy of a BCL-2 converting peptide, NuBCP-9. Nanoscale 6(23):14473–14483
22. Prevo B, Esakoff S, Mikhailovsky A, Zasadzinski J (2008) Scalable routes to gold nanoshells with tunable sizes and response to near-infrared pulsed laser irradiation. Small 4:1183–1195
23. Kimmel CB, Ballard WW, Kimmel SR, Ullmann B, Schilling TF (1995) Stages of embryonic development of the zebrafish. Dev Dyn 203(3):253–310
24. Schindelin J, Arganda-Carreras I, Frise E, Kaynig V, Longair M, Pietzsch T et al (2012) Fiji: an open-source platform for biological-image analysis. Nat Methods 9(7):676–682
25. Wehmas LC, Tanguay RL, Punnoose A, Greenwood JA (2016) Developing a novel embryo–larval zebrafish xenograft assay to prioritize human glioblastoma therapeutics. Zebrafish 13:317–329
26. Chakraborty C, Sharma AR, Sharma G, Lee S-S (2016) Zebrafish: a complete animal model to enumerate the nanoparticle toxicity. J Nanobiotechnol. https://doi.org/10.1186/s12951-016-0217-6
27. Liu J, Liu Y, Bu W et al (2014) Ultrasensitive nanosensors based on upconversion nanoparticles for selective hypoxia imaging in vivo upon near-infrared excitation. J Am Chem Soc 136:9701–9709
28. Liu H-Y, Wu P-J, Kuo S-Y et al (2015) Quinoxaline-based polymer dots with ultrabright red to near-infrared fluorescence for in vivo biological imaging. J Am Chem Soc 137:10420–10429